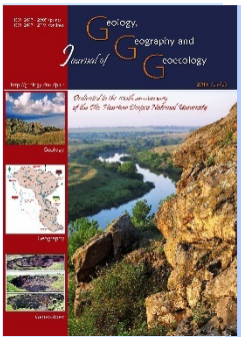

Journal of Geology, Geography and Geoecology

Journal home page: **geology-dnu-dp.ua**

ISSN 2617-2909 (print)
ISSN 2617-2119 (online)

Journ.Geol.Geograph. Geoecology, 27(3), 453-465
doi:10.15421/111869

Modeling the distribution of land surface temperature for Bystrytsia river basin using Landsat 8 data

Kovalchuk I.P.[1], Mkrtchian O.S.[2], Kovalchuk A.I.[3]

[1]*National University of Life and Environmental Sciences of Ukraine, Kyiv, Ukraine,e-mail: kovalchukip@ukr.net*
[2]*Ivan Franko National University of Lviv, Lviv, Ukraine,e-mail:alemkrt@gmail.com*
[3]*Taras Shevchenko National University of Kyiv, Kyiv, Ukraine,e-mail:kovalchuk94a@gmail.com*

Received 25.09.2018;
Received in revised form 28.10.2018;
Accepted 07.11.2018

Abstract. Development of accurate and practicable methods of land surface temperatures (LST) mapping has benefits for a range of scientific and practical applications. The paperconsiders mapping of LST for the Bystrytsia river basin located in Western Ukraine using Landsat 8 imagerywith two thermal infrared bands, which capture emissivity values closely related to land surface temperature (LST).Three multispectral images referring to different seasons (autumn, winter and summer) were used in the study. The method of LST estimation consists of several successive steps. After preprocessing (clipping, masking, and re-projecting), the images were converted from digital numbers to top of atmosphere spectral radiance,and then – to brightness temperature.However, the brightness temperature differs from LST due to emissivity of land surface being different from that of ideal blackbody.The emissivity can vary significantly with vegetation, surface moisture and surface roughness, and can be approximately estimated from land surface reflectivity at red and near-infrared spectral ranges.Estimated values of LST were compared with measurements of Ivano-Frankivsk state weather station, showing rather good compliance for all the three scenes.Obtained estimates of LST show some regularities of its spatial distribution, which also vary significantly from season to season.All the three scenes show conspicuous vertical gradient in LST; summer and autumn scenes are also characterized by significant local variability in LST due to different land cover types (e.g., urban development, forests, different agricultural lands), whereas in winter, differences in LST for mountainous slopes of different aspects appear to be more pronounced. Graphs of LST change with elevation have a parabolic form: sharper decrease of LST is typical for lower elevations, while the vertical LST gradient decreases above 700–1000 m a.s.l.

Keywords: land surface temperature, Landsat, Carpathians, Bystrytsia river basin, land surface emissivity, NDVI

Моделювання розподілу температури підстильної поверхні для басейну р. Бистриця за даними знімків Landsat 8

Ковальчук І. П.[1], Мкртчян О. С.[2],Ковальчук А. І.[3]

[1]*Національний університет біоресурсів і природокористування України, м. Київ.e-mail: kovalchukip@ukr.net*
[2]*Львівськийнаціональнийуніверситетіменіівана Франка, м. Львів,e-mail:alemkrt@gmail.com*
[3]*Київськийнаціональнийуніверситетімені Тараса Шевченка, м. Київ,e-mail:kovalchuk94a@gmail.com*

Анотація. Розвиток точних та практично зручних методів картування температури підстильної поверхні (ТПП) є корисним для низки наукових галузей та прикладних застосувань. У статті розглянуті питання картування ТПП для басейну р. Бистриці, розташованої у західній частині України, з використанням космознімків Landsat 8, які включають два термальних інфрачервоних діапазони, що реєструють значення випромінювання, тісно пов'язані з ТПП.З веб-порталу USGS було скачано три мультиспектральні знімки, які отримано у три різні сезони року (осінь, зима та літо). Метод обрахунку ТПП, описаний та використаний у дослідженні, складається з кількох послідовних кроків. Після попередньої обробки, яка складалась з обрізки, маскування та перепроектування знімків, вони були перетворені з умовних цифрових значень у значення випромінювання на верхній межі атмосфери, а далі – у значення яскравісної температури. Проте, яскравісна температура відрізняється від ТПП, оскільки випромінювальна здатність земної поверхні відрізняється від випромінювальної здатності абсолютно чорного тіла. Випромінювальна здатність може суттєво змінюватись в залежності від характеру рослинності, зволоження та шорсткості поверхні, але в першому наближенні може бути оцінена за значеннями відбивальної здатності поверхні у червоному та ближньому інфрачервоному діапазонах спектру. Оцінені значення ТПП булиспівставлені зі значеннями, вимі-

ряними на метеостанції Івано-Франківськ, при цьому виявлено достатньо добру відповідність для всіх трьох випадків. У просторовому розподілі обрахованих значень ТПП встановлено низку закономірностей, які до того ж відрізняються за сезонами року. В усіх трьох випадках спостерігався виражений вертикальний градієнт у значеннях ТПП. Літній та осінній розподіли також характеризувались значною локальною мінливістю в ТПП, пов'язаною з різними наземними покривами (напр., міською забудовою, лісами, різними сільськогосподарськими угіддями), тоді як зимовий розподіл ТПП характеризувався більш вираженими експозиційними відмінностями гірських схилів. Графіки зміни ТПП з висотою мають параболічну форму: більш різке зменшення ТПП з висотою характерне для нижчих висотних рівнів, тоді як вище 700–1000 м над рівнем моря її висотний градієнт зменшується.

Ключові слова: температура підстильної поверхні, Landsat, Карпати, басейн р. Бистриця, випромінювальна здатність земної поверхні.

Introduction. Thermal regime of an area isan important constituent of its natural conditions, possessing large ecological significance and influencing a set of hydrological and geomorphological processes. Land surface temperatures (LST) measurements allow to infer energy balance components of a given region that are essential for understanding ecosystem processes as well as for estimating the componentsof hydrological cycle. LSTalso influence the suitability of area for cultivation of heat-lovingplants, forest productivity, prevalence of pests and plant diseases, the set of touristic and recreational activities like skiing, swimming, etc. Detailed study and mapping of thermal characteristics utilizing various sources of data are thus of great importance for the tasks of territorial planning, nature conservation, urban heat analysis, precision agriculture, forestry, resort activity, to name just a few. Thence the importance and practical relevance of the study topic.

Detailed spatial analysis of thermal conditions is not a simple task, as regards both the data acquisition and the data processing methodology. The most reliable source of climatic data are weather stations with sufficiently long uninterrupted observation series. However, the network of such weather stations in many countries is rather patchy and tenuous, as in the case ofUkraine where weather stations located in Carpathian region cannot cover the respective variability of climatic conditions Another possibility is the study of temperature regime using automatic ground sensors (data loggers); however, this methods allows studying only inside small local areas or along relatively short profiles, in a limited number of observation points corresponding to the number of available sensors. Yetanother possibility lies in building models that allow to interpolate weather stations data in space, thus creating continuous climatic surfaces. Spatial interpolation can be carried out using geostatistical methods, based on the statistical analysis of the spatial variability of temperature fields; using regression models that characterize relationships between the temperature and its spatially distributed predictors (e.g., elevation field and morphometric terrain characteristics); or the combination of regression and geostatistical approaches. The latter approach is the most general and can take form e.g. of building the regression model first and then interpolating the residuals of regression by means of geostatistical method (Mkrtchian, Shuber, 2009).However, the prediction accuracy of this approach can be low when the network of weather stations is sparse,leading to poor model predictions for the places too remote from samples (weather stations) in geographic or feature spaces (e.g. for highlands represented with few weather stations).

New possibilities for the analysis and mapping of thermal conditions have opened with the emergence and advancement of modern remote sensing methods. While land surface like any heated object emits thermal radiation in far (thermal) infrared area of electromagnetic spectrum, the total energy radiated per unit surface area per unit time being proportional to the fourth power of the body's thermodynamic temperature, the emissivity of land surface inthe far infrared can be used to infer its temperature.The detailed theoretical review of the issue of the retrieval of LST from space measurements, the classification and comparison of different methods for retrieving LST from satellite data, and the methods of validation of satellite-derived LST can be found in (Li et al., 2013).

Some of the modern remote sensing platforms keep sensors that perceive and measure far infrared radiation. The earliest and longest-runningLandsat program for acquisition of Earth satellite imagery began employing such sensors since the launch of Landsat 3 satellite in 1978, but this instrument failed shortly after the satellite was deployed into orbit. Starting from Landsat 4 (launched in 1982), Thematic Mapper (TM) sensors are carried on board, featuring a thermal infrared band (Band 6) that has a maximum spatial resolution of 120 m.Landsat 7 (launched in 1999) keeps an Enhanced Thematic Mapper Plus (ETM+) sensor, its Band 6 acquired at 60m resolution. Lastly, the most recent Landsat 8 satellite (launched in February 2013)features the Thermal Infrared Sensor (TIRS) built by the NASA Goddard Space Flight Center, that collects data for two long wavelength infrared bands with 100 m resolution(NASA, 2018).

The remotely sensed data from Landsat satellites with global coverage are now distributed free of charge, which makes it a promising data source for mapping the distribution of LST. While it is still impossible to directly infer air temperatures from remotely sensed data, LST can be a good proxy for the former, as well as for the temperatures of upper soil layers. Landsat satellites also carry sensors for measuring the reflectance of land surface in visual and near-infrared spectral bands: this can be used to analyze the characteristics of land surface that influence its emissivity (propensity to emit more or less far infrared radiation for any given temperature).

The purpose of this study is to research into the possibility of using remotely sensed imagery to analyze and map the spatial distribution of LST, on an example of Bystrytsia river basin located in western part of Ukraine. As the spatial distribution of LST obviously differs by seasons throughout the year, Landsat 8 images taken in different seasons should be jointly analyzed to obtain more clear picture.

Researchers from many countries have recently elaborated methods to derive LST form Landsat 8 "thermal" bands. Examples can be given of studies from India (Jeevalakshmi et al., 2017; Anandababu et al., 2018), Turkey (Oguz, 2017), Brazil (de Jesus, Santana, 2017). Brazilian researchers obtained the estimation of LST for semi-arid area in the state of Sergipe using two images obtained in the rainy and dry seasons, subsequently comparing the statistical properties of the two output temperature surfaces (de Jesus, Santana, 2017). Indian researchers have taken similar approach, analyzing images taken in the rainy and dry seasons for study areas in Andhra Pradesh state (Jeevalakshmi et al., 2017) and Tamil Nadu state in southern India (Anandababu et al., 2018).

All these researches applied a similar methodology, described in detail in (Xiaolei, Xulin, Zhaocong, 2014). In this work, three different methods for LST derivation from Landsat 8 TIRS data have been compared, including the radiation transfer equation-based method, the split-window algorithm and the single channel method.Validation results for the investigated sites and scenes showed that the LST derived by the radiation transfer equation-based method using Band 10 has the highest accuracy among all the reviewed methods (Xiaolei, Xulin, Zhaocong, 2014). In the another research (Sobrino, Jimenez-Munoz, Paolini, 2004) this method gave better results than some alternative algorithms for the retrieval of LST from Landsat TM 5 data, assessed by Root mean square deviation (RMSD). Thus, radiation transfer method was the one applied in above-cited empirical studies.

Material and Methods. The study areacomprises the basin of Bystrytsia river with an area of 2500 км^2, located in central part of Ivano-Frankivsk oblast of Ukraine. Bystrytsia is the left tributary of Dnisterriver that flows into Black sea. Despite its small area, the Bystrytsiabasin is characterized by a diversity of natural conditions, land use types, and characteristics of land surface. Its north-eastern part is mainly covered by wide terraced piedmont valleys of the rivers BystrytsiaSolotvynska, BystrytsiaNadvirnyanska and Vorona. In the south-western and southern parts of the basin, there are low and medium mountains of the Carpathians. Altitudes vary from 201 m (areas near river mouth) to 1836 m (summit of mt. Syvulia Velyka) (Fig. 1). Climate is moderate and moderately continental, with cool summers, mild winters with unstable snow cover, and frequent changes in weather. Average annual temperature is around +8°C in low northern part, and decreases to +2-3°C in the highest parts of the mountains. Annual precipitation is 650–700 mm in the lowlands and increases to 1000 mm and more in mountainous part of the basin.

As to the land cover structure in the basin area, its north-eastern (lowland valley) part is mainly covered by agricultural lands, with small patches of broad-leafed forests among them (Fig. 2). There are also some urbanized areas, mostly in and around Ivano-Frankivsk city (its urban area 84 km^2), in Nadvirna and Tysmenytsia towns, and in some large villages. In the mountainous south-western part of the basin forested lands prevail: mixed forests in low mountains and mostly coniferous ones higher up. The highest crests and slopes of Horhany massif are covered with stone placers and taluses.

Landsat 8 imagery has been used as the main data source for the study. Landsat 8 carries two push-broom instruments: the Operational Land Imager (OLI) and the Thermal Infrared Sensor (TIRS), that jointly produce a multispectral image consisting of 11 spectral bands. OLI collects nine spectral bands including a pan band: bands 1–4 correspond to visible part of the electromagnetic spectrum, bands 5–7 and 9 – to near-infrared and shortwave infrared regions of the spectrum (all of these have a spatial resolution of 30 m); band 8 is panchromatic, taking images in wide visible wavelength range (0,503–0,676 μм) with 15 m spatial resolution. These bands allow to obtain various kinds of information on the characteristics of land surface, including vegetation cover. The TIRS instrument collects two spectral bands for the far infrared wavelengths covered by a single band on the previous TM and ETM+ sensors:band 10 (TIRS 1, 10.6–11.19 μm) and band 11 (TIRS 2, 11.5–12.51 μm), both with 100 m spatial resolution (NASA, 2018).

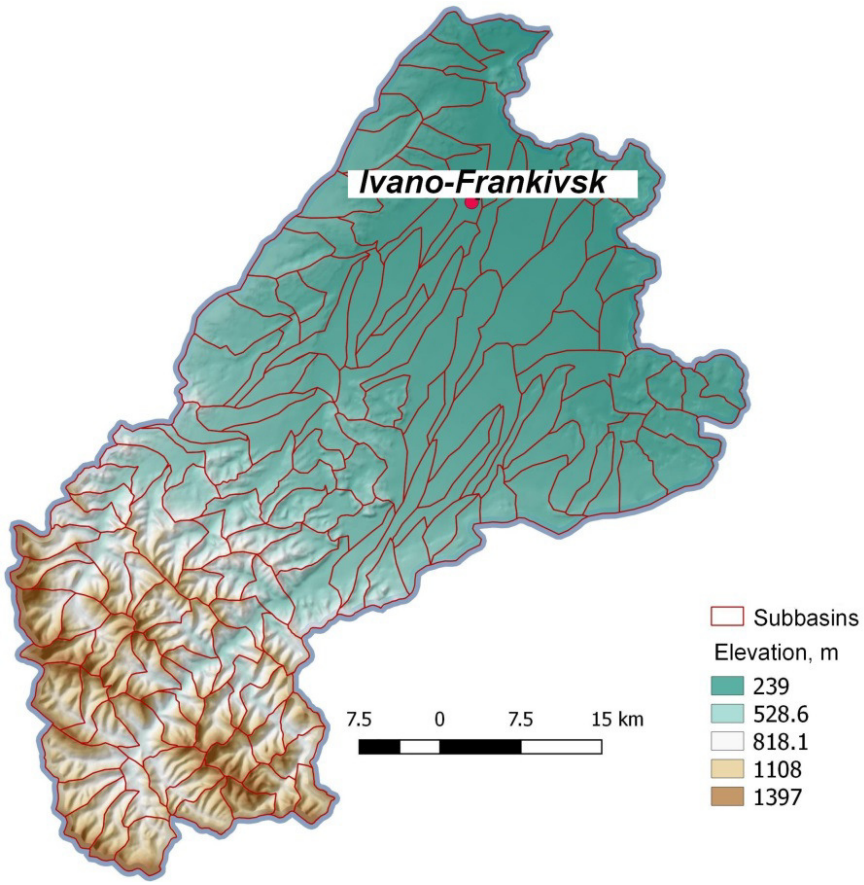

Fig. 1. Bystrytsia river basin and its terrain.

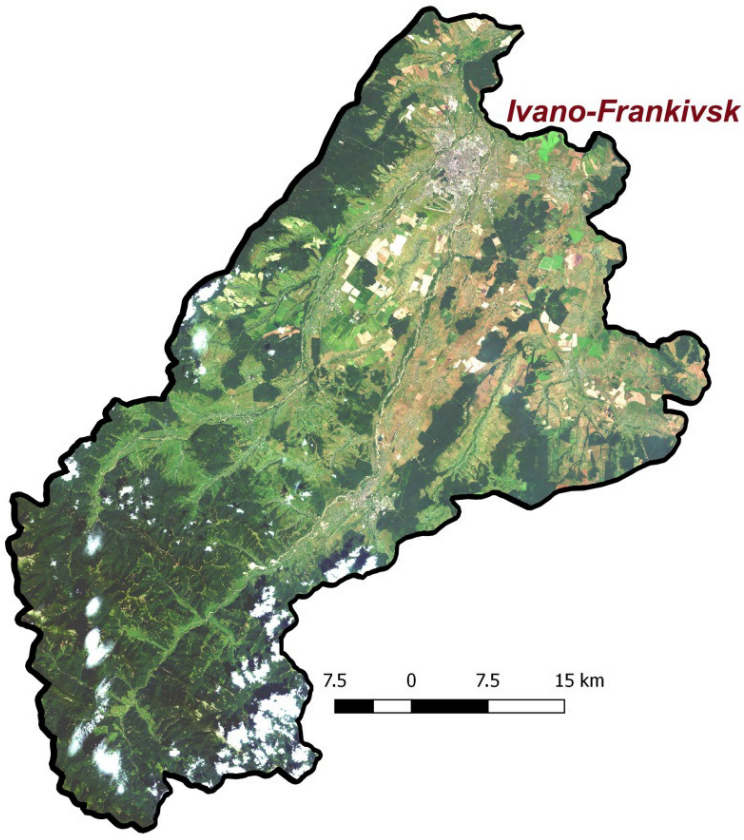

Fig. 2. Bystrytsia river basin and its land cover (Landsat composite image for August 10, 2016).

As the Landsat 8 satellite acquires images of the entire Earth every 16 days, there is a possibility to use them not only to map the static distribution of certain phenomena, but also to analyze their dynamical properties. For instance, long wavelength infrared bands of images acquired in different seasons of the year allow to study seasonal differences in the spatial distribution of LSTand its driving factors. However, the limiting factor is the considerable cloud cover in many images, which effectively limits the amount of information that could be extracted from image.

To cover the annual variability in LST conditions, it is expedient to use images taken in different seasons of the year. For the purpose of our study, Landsat 8 images has been downloaded from USGS web portal (https://earthexplorer.usgs.gov). From scores of available images for the area, three were chosen based on criteria of small percentage of cloud cover, relatively recent acquisition data (to minimize land cover changes between images), and different seasons of the year. The chosen images refer to following dates: October 5, 2013; February 13, 2015; August 10, 2016. The first one characterizes the thermal conditions close to average for the year, while the second and the third – the typical conditions for winter and summer day. All the images were taken at similar local time, contributing to comparability of their reflectance characteristics (Table 1).

Table 1. General characteristics of the scenes of Landsat 8 images used in the study.

Date	Local time	Sun height	Cloud cover percentage of the scene	Air above-ground temperature (Ivano-Frankivsk weather station)
2013, October 5	12:16	35,07˚	6,73%	9 °C
2015, February 13	11:14	24,99˚	0,67%	1.4 °C
2016, August 10	12:14	53,17˚	7,89%	26 °C

Data preprocessing of these images consisted of their clipping to the contours of the basin, and the masking out of cloud-covered areas, by means of special Band quality assessment (BQA) raster layer supplied with the Landsat 8 images. The images were projected to a Universal Transverse Mercator (UTM) coordinate system, datum WGS84, zone 34N, for more accurate spatial analyses. While visual and near-infrared spectral bands were used for refining the temperature data (see below), their spatial resolution (30 m) being different from that of TIRS bands (100 m), they had to be led to common resolution; 50 m has been chosen as a "compromise" value.

As an auxiliary data source, SRTM Digital elevation model (DEM) has been used with 30 m spatial resolution (Farr et al., 2004) to assist in data visualization (see Fig. 1) and to analyze the relationships between the elevation and the estimated LST.Data processing has been performed using open source GIS software: SAGA (mainly for data preprocessing: clipping, masking and resampling) (Conrad et al., 2015), and QGIS – mainly for raster map algebra operations and data visualization(https://www.qgis.org).

The general scheme of LST derivation according to methodology described in (Xiaolei, Xulin, Zhaocong, 2014) consists of several steps (see Fig. 3).The first step is the conversionof the Digital Numbers (raw values) of bands to at-sensor spectral radiance(TOA spectralradiance,Watts/ (m^2 * sr * μm)). This step is pretty simple and applies the formula:

$$L_\lambda = \mathrm{ML}^* Qcal + \mathrm{AL} \qquad (1)$$

whereL_λ– TOA spectral radiance (watts/(m^2*ster*μm)), *Qcal* = quantized and calibrated standard product pixel values (Digital Numbers), ML and AL – respectively, band specific multiplicative (ML) and additive (AL) rescaling factors, whose values are contained in the image metadata (RADIANCE_MULT_BAND_n and RADIANCE_ADD_BAND_n, where n is the band number).

At the second step, the brightness temperature is estimated using formula:

$$BT = \frac{K_2}{\ln(\frac{K_1}{L_\lambda}+1)} - 273.15 \qquad (2)$$

where*BT*is the brightness temperature,K_1 and K_2 are the thermal constants of TIR bands (also contained in the image metadata),L_λ – TOA spectral radiance, 273.15 – a constant to convert the results from Kelvin to Celsius scale. One can stop here and use the calculated brightness temperature as an approximation of LST, as it is done e.g. in (Vyshnevskyi, Shevchuk, 2017). However, the intensity at which land surface emits thermal radiation is not the same as that of an ideal blackbody with the same temperature. Theemissivity of land can varysignificantly with vegetation, surface moisture and surface roughness(Glenn et al., 2008). Thus, it should be accounted for to acquire more accurate measure of LST. It can be done using formula (Xiaolei, Xulin, Zhaocong, 2014):

$$LST = \frac{BT}{1+(BT*\lambda*\frac{\ln \varepsilon}{\rho})} \qquad (3)$$

where BT is the brightness temperature (2), λ is the average wavelength of band on which data it was calculated (10.6 – 11.19 micrometers for Band 10 and 11.5 – 12.51 for Band 11), ρ ≈ 0.0144 is the

coefficient based on physical constants: $\rho = h\frac{c}{\sigma}$, where h is Plank's constant ($6.626\ 10^{-34}$), σ is the Boltzmann constant ($1.38\ 10^{-23}$ J/K), and c is the velocity of light ($3\ 10^{8}$ m/s). ε in this formula relates to land surface emissivity – a proportionality factor that scales blackbody radiance (Planck's law) to predict emitted radiance, the efficiency of transmitting thermal energy across the surface into the atmosphere (Sobrino, Jimenez-Munoz, Paolini, 2004; Sobrino et al., 2008).According to (Sobrino, Jimenez-Munoz, Paolini, 2004) and (Mallick, Kant, Bharath, 2008)it can be calculated as:

$$\varepsilon_\lambda = \varepsilon_{v\lambda} P_v + \varepsilon_{s\lambda} (1 - P_v) + C \quad (4)$$

where ε_v and ε_s are the vegetation and soil emissivities respectively, P_v – is the proportion of area covered with vegetation as opposed to bare soil and artificial surfaces, and C is the surface roughness that in the absence of information can be taken as a constant value of 0.005 (Sobrino et al., 2008). Information on proportion of different land cover types can be obtained from analysis of visible and near-infrared image bands. Well-fit tool for this purpose is Normalized Difference Vegetation Index (NDVI) introduced in 1973 and since then extensively applied in the various fields for the vegetation and landscape analyses of remotely sensed data (Glenn et al., 2008; Mkrtchian, 2016). It is calculated by the formula:

$$NDVI = \frac{NIR - RED}{NIR + RED} \quad (5),$$

where *RED* and *NIR* are the reflectance values in red and near-infrared spectral ranges, respectively. It has been shown that the values of this index correlate closely with the wide set of vegetation characteristics, including leaf area index that can serve a proxy to the share of vegetation-covered land surface types(Glenn et al., 2008). *RED* and *NIR* values in formula (5) can be derived from, respectively, Band 4 and Band 5 of the same multispectral Landsat 8 image which TIR band have been used earlier in estimating *BT*.

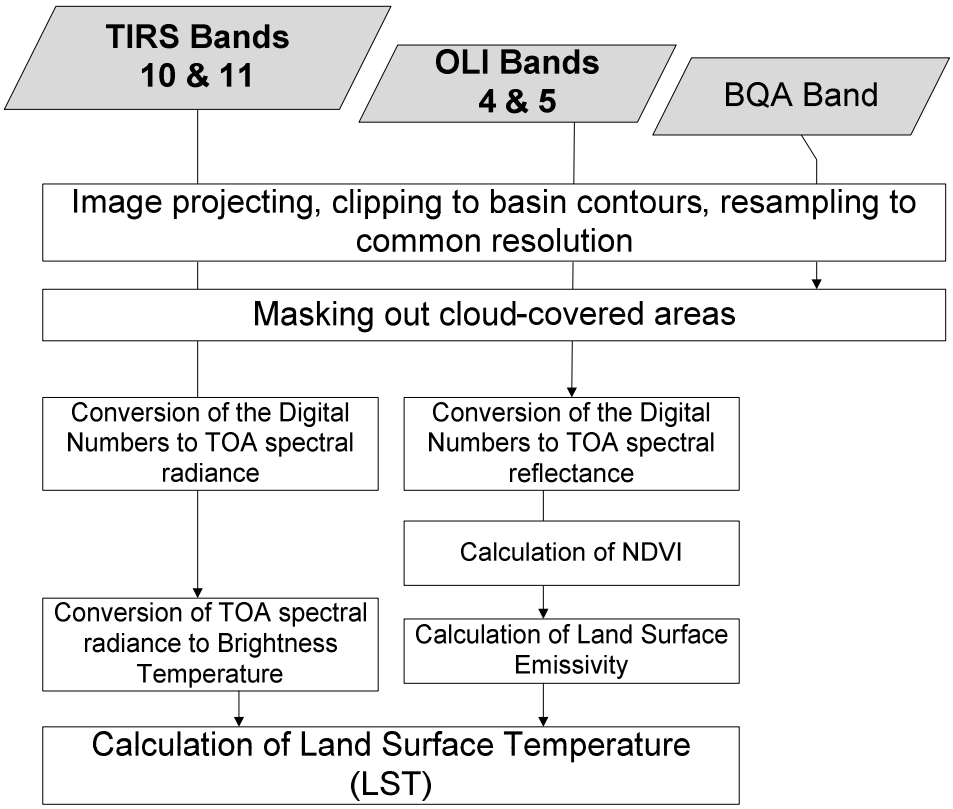

Fig. 3. Flowchart of the LST retrieval from Landsat 8 images.

There are different approachesto relate NDVIto land surface emissivity (Sobrino, Jimenez-Munoz, Paolini, 2004; Sobrino, Raissouni, 2010; Jeevalakshmi, Narayana, Manikiam, 2017; de Jesus, Santana, 2017). In general, these approaches are based on NDVI Thresholds Method (Sobrino, Jimenez-Munoz, Paolini, 2004; Sobrino et al., 2008), which envisages the establishment of two "threshold" NDVI values. NDVI = 0.2 or lower imply the bare soil, NDVI = 0.5 or higher imply the vegetation cover, and its values in between 0.2 and 0.5 relate to some proportion between the two in land cover structure. While land surface emissivity also depends on surface roughness, it is much easier to disregard its spatial heterogeneity and to replace it with a constant. Recommended value of emissivity for surfaces fully covered with vegetation is 0.99 (Sobrino et al., 2008). Emissivity for bare surfaces

vary depending on character of soil and generally stay in linear relationship with emissivity in the red region of spectrum (Sobrino et al., 2008). For simplicity, the constant value is used in most works, yet the specific value in above-cited works vary from 0.966 in (Jeevalakshmi, Narayana, Manikiam, 2017) and 0.971 in (Oguz, 2017) to 0.986 in (Anandababu, Purushothaman, Suresh, 2018) and (de Jesus, Santana, 2017). Thus, the value 0.977 can be taken as an averaged best guess at a first approximation. And if NDVI value is between 0.2 and 0.5, the land cover is assumed to be a mix of bare ground and vegetation, with their proportion reflected by NDVI. In these cases, ε is calculated as:

$$\varepsilon = 0.99\frac{NDVI-0.2}{0.3} + 0.977\frac{0.5-NDVI}{0.3} \qquad (6)$$

After this, ε (land surface emissivity) is substituted in (3) and the resultant value of LST is thus calculated. The general scheme of LST retrieval from Landsat 8 image bands is shown on flowchart (Fig. 3).

Results and Discussion. Let's first illustrate the results of the calculation of land surface emissivity. NDVI calculated for summer image (Fig. 4) shows the highest values for areas covered with deciduous forests (located mainly in piedmont areas in central and western parts of the basin), the mediocre values for coniferous forests predominant in mountainous south-western part of the basin, and the lowest values for urban areas, open water, and some arable lands.

The similar pattern is revealed by the distribution of land surface emissivity (Fig. 5). It was taken to amount to 0.977 for places with NDVI < 0.2, to 0.99 for places with NDVI > 0.5, while for places with NDVI between 0.2 and 0.5 it was calculated by formula (6). Where the land surface emissivity is low enough, the brightness temperature calculated with (2) can be noticeably smaller than real LST value (Fig. 6).

The same parameters were calculated for other two images (not shown here), their spatial distribution being slightly different with that shown in Fig. 5–6.The final maps of LST distribution for the three above-mentioned scenes are given in Fig. 7–9.

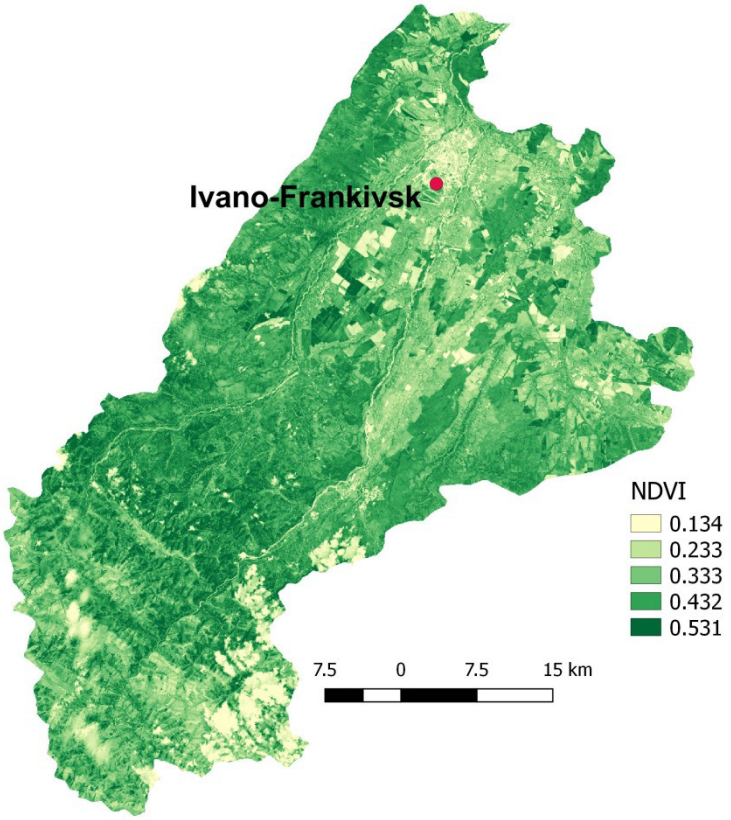

Fig. 4. NDVI values calculated for August 10, 2016, by formula (5).

To verify the accuracy of obtained LST estimations, they were collated with data recorded for Ivano-Frankivsk weather station (the single state weather station located in this basin) for the same date and time (Tab. 2). As can be seen, the discrepancies for all the three cases are small (less than 1°C) and comparable with these obtained by other researchers. In the above-cited research (Jeevalakshmi et al., 2017) the obtained results were compared to air temperature measurements taken

by 14 automatic weather stations, having found the standard deviation as 1.79°C for the first case (the dry season) and 1.02°C for the second case (the wet season). The authors attributed these deviations to the generalized 100 m resolution image estimations being superimposed with weather stations point measurements, and also to the possible differences between LST and air temperatures measured 2 m above the surface. In the study (Sobrino, Jimenez-Munoz, Paolini, 2004), the comparisonbetweenthe ‘‘insitu’’ LSTmeasurements andthevalues obtainedfromtheRadiativetransferequationmethod similar to that used in our study, showed anRMSD value of 0.6 K, with the largest discrepancies (1.22 K) observed for light soils with few vegetation.

Table 2. Collating weather station data for Ivano-Frankivsk with LST estimated from Landsat 8 images.

Date	Local time	Air above-ground temperature, ˚C (measured in weather station)	Land surface temperature, ˚C (calculated from Landsat 8 imagery)	Air pressure, hPa	Relative humidity, %	Wind speed, km/h
05.10.2013	12:00	9	9.5	1029	54	2
13.02.2015	11:00	1.4	1.6	1027	72	0
10.08.2016	12:00	26	26.5	1014	61	1

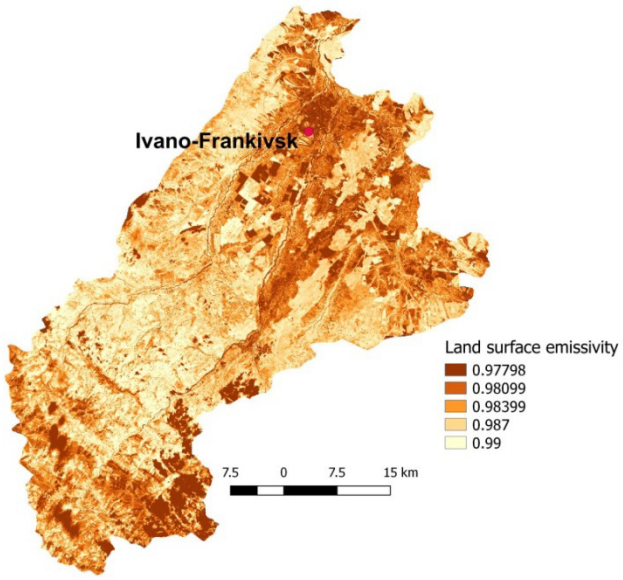

Fig. 5. Land surface emissivity values calculated for August 10, 2016, by formula (6).

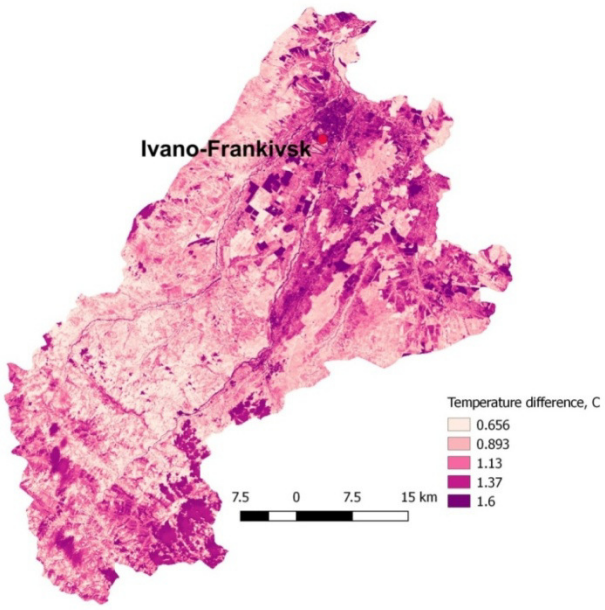

Fig. 6. Differences between LST calculated with formula (6) and brightness temperature, calculated for August 10, 2016.

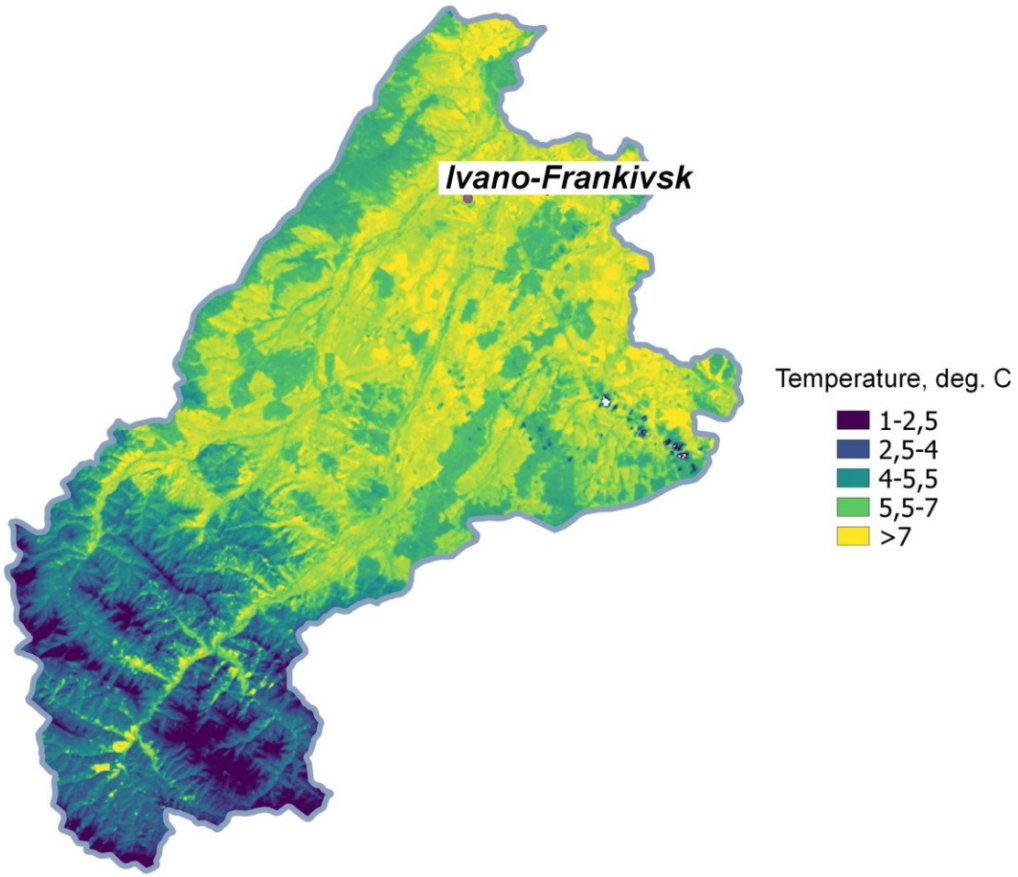

Fig. 7. Distribution of LST for the Bystrytsia basin for October 5, 2013.

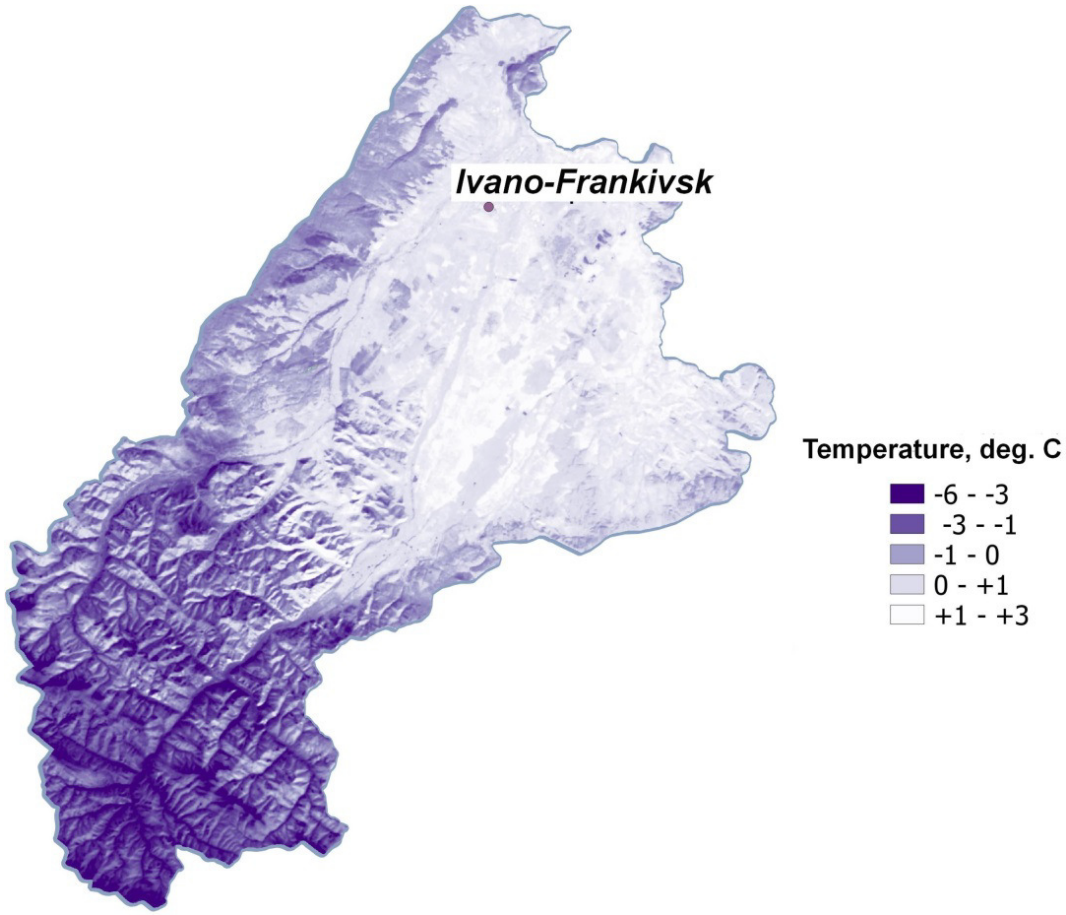

Fig. 8. Distribution of LST for the Bystrytsia basin for February 13, 2015.

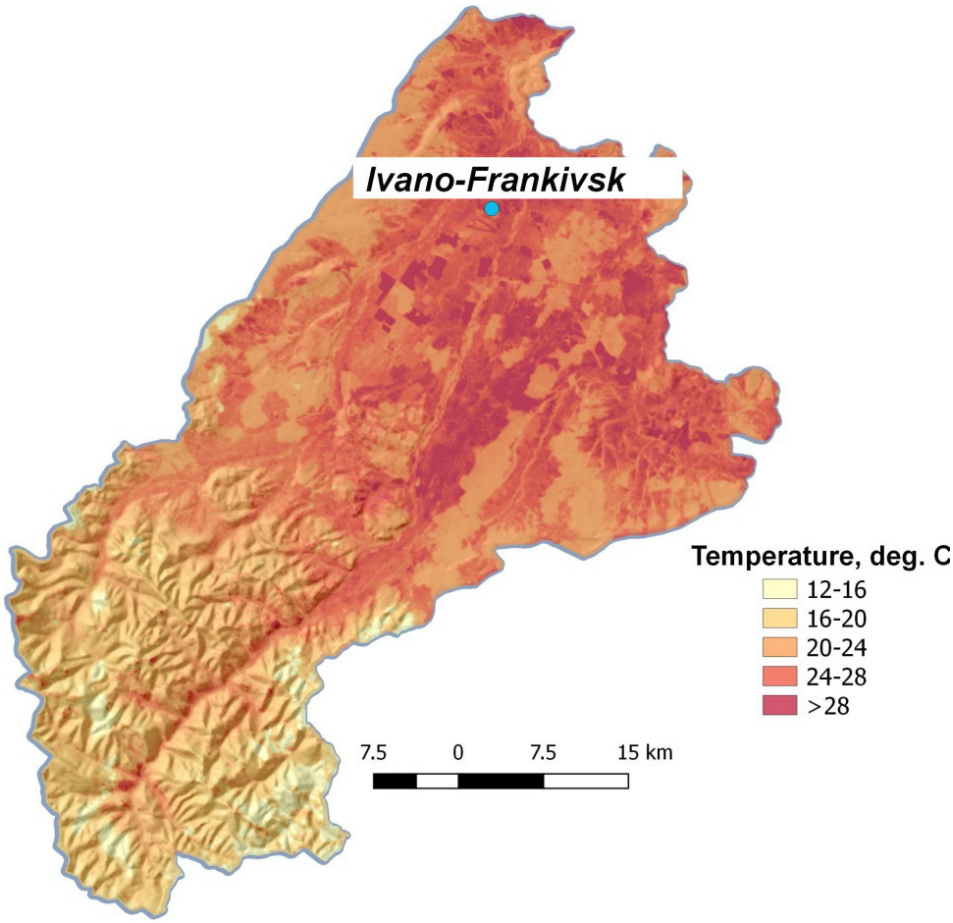

Fig. 9. Distribution of LST for the Bystrytsia basin for August 10, 2016.

As seen from the obtained maps (Fig. 7–9), the distributions of LST values obtained for different seasons have some common features, as well as some differences. Temperatures in lowland northern part of the basin are substantially higher than in its mountainous part:differences range from 5–8°C for autumn and winter scenes to more than 10°C for summer one. For autumn and summer scenes, there are pronounced differences in LST between different land cover types: e.g. forested areas are significantly cooler than arable land and build-up areas. It is in accordance with a statement from (de Jesus, Santana, 2017), that cite a set of works on semi-arid areas of north-eastern Brazil showing that the changes in NDVI values associated with the different land uses and states of vegetation have been inversely related with the LST values: more vigorous vegetation is generally characterized by lower LST.In the winter, the differences between slopes of different aspect become pronounced in mountainous areas, mainly due to lower position of sun. Narrow valley bottoms in the mountainous part are more heated than surrounding slopes in summer and autumn, while in winter they are the coldest part of the area, probably because of shading and prevalence of inversions.

Finally, let's look into the possibilities to analyze the estimated LST spatial distributions and its factors by applying regression models that include factors and variables affecting these distributions. While it is not a direct topic of this research, this was illustrated by taking elevation (derived from SRTM DEM) as single independent variable, and looking on how changes in elevation affect average LST for the given elevation. For this purpose, R language and environment for statistical computing has been applied. Polynomial regression models with cubic term and elevation as an independent variable have been built with R lm() function for three scenes, and visualized using R plotting capabilities (Fig. 10–12). While there is a general tendency of LST to decrease with elevation, the rate and form of this relationship seems to vary with season. The rate of decrease is highest for elevations below 1000 m a.s.l., while higher up it remains practically constant (in winter LST practically ceases to increase already above 600–700 m). Trend line above 1500 m is unreliable here due to small sample size in this basin.

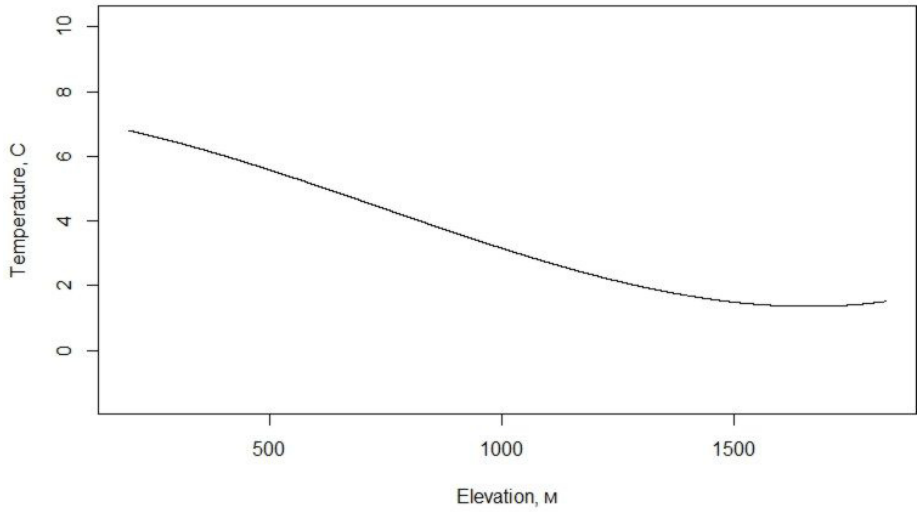

Fig. 10. Average LST change with elevation, 05.10.2013.

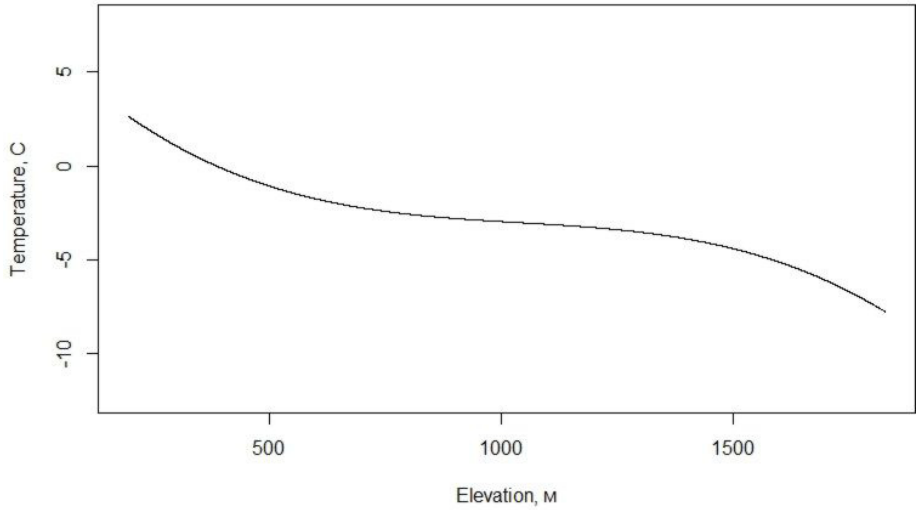

Fig. 11. Average LST change with elevation, 13.02.2015.

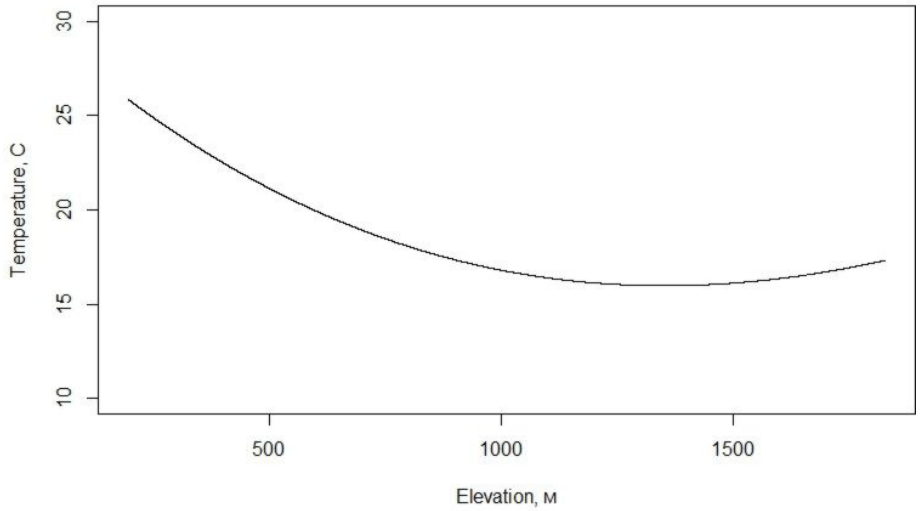

Fig. 12. Average LST change with elevation, 10.08.2016.

Conclusion. The multispectral images containing TIRS bands can serve a valuable data source for the mapping of LST. Landsat 8 multispectral images containingtwo TIRS bands can be effectively used to map LST distribution for different regions and time periods. However, the procedure of derivation of LST values from images is not straightforward and provides for several consecutive steps. Thus, the emissivity of land surface (the intensity at which it emits thermal radiation) at the given temperature can vary significantly with vegetation, surface moisture and surface roughness, and should be accounted for when converting brightness temperature into LST. One of the methods of assessing

emissivity is based on the NDVI values, that can be derived from the red and near-infrared bands of the same multispectral Landsat 8 imagewhich TIRS bands have been used in estimating brightness temperature.

The application of the radiation transfer equation-based method of LST derivation to the images for Bystrytsia river basin area obtained in different seasons of the year allowed to analyze its spatial distribution and its seasonal variability.While all the three scenes show conspicuous vertical gradient in LST, summer and autumn scenes are also characterized by significant local variability in LST due to different land cover types (e.g., urban development, forests, different agricultural lands), whereas in winter scene differences in LST for mountainous slopes of different aspects are more pronounced.

Estimations of LST can be improved by considering atmospheric effects, and by using more precise algorithms to account for land surface emissivity. The question remains as to whether apply only data of one of the two Landsat 8 TIRS bands in the derivation of LST, or to combine data from both bands 10 and 11, trying to capitalize on self-cancellation of their errors by averaging. In (Xiaolei, Xulin, Zhaocong, 2014) it is claimed that RMSE of LSTs obtained from single band 10 is slightly smaller than that in the case of also using band 11. The stated cause of this is the larger calibration uncertainty associated with band 11, that is more affected by the water vapor continuum absorption (Xiaolei, Xulin, Zhaocong, 2014; Coll, 2012). Thus, different researchers take different choices on this: above-cited works of (Jeevalakshmi, Narayana, Manikiam, 2017) and (Oguz, 2017) rely solely on Band 10 in their derivation of LST, while (Anandababu, Purushothaman, Suresh, 2018) and (de Jesus, Santana, 2017) derived their estimates of LST by averaging data from bands 10 and 11. In general, the reason for the inclusion of second TIR band in the Landsat 8 image band set has been to enable applying a split-window method, that relies on calculatingthe differencesin TIR radiance measurements at twodifferent wavelengths to estimate the radiance attenuation foratmospheric absorption.If the future satellites like Landsat 9 provide the well-calibrated data for both TIR bands, split-window method for LST retrieval could fare no worse thanradiation transfer method.

Calculating LST values for different river basins and different times of the year with the same method could allow to make inferences about the factors and regularities of their spatial distribution. It would also be helpful to automate this process by creating algorithms that make it through the steps of the process of the LST derivation (Fig. 3), from the input image to the output LST map. Yet it should be remembered that the estimation of LST from satellite data is dependable on current weather condition and is obstructed in periods of significant cloud cover. It is also temporarily bound by the scheduled time of satellite flyby. Thus if the obtained LST data are summarized, the obtained inferences will contain the ensuing biases that should be acknowledged and accounted for.

References

Anandababu, D., Purushothaman, B.M., Suresh, B.S., 2018.Estimation of Land Surface Temperature using LANDSAT 8 Data.International Journal of Advance Research, Ideas and Innovations in Technology.4 (2), 177–186.

Coll, C.; Caselles, V.; Valor, E.; Niclòs, R., 2012. Comparison between different sources of atmospheric profiles for land surface temperature retrieval from single channel thermal infrared data. Remote Sens. Environ. 117, 199–210.

Conrad, O., Bechtel, B., Bock, M. et al., 2015. System for Automated Geoscientific Analyses (SAGA) v. 2.1.4.Geosci. Model Dev. 8, 1991–2007.

de Jesus, J.B., Santana, I.D.M., 2017. Estimation of land surface temperature in Caatinga area using Landsat 8 data.Journal of Hyperspectral Remote Sensing. 7, 150–157.

Farr, T.G. et al., 2004. The Shuttle radar topography mission. Rev. Geophys. 45 (2), RG2004.

Glenn, E.P., Huete, A.R., Nagler, P.L., Nelson, S.G., 2008. Relationship between remotely-sensed vegetation indices, canopy attributes and plant physiological processes: what vegetation indices can and cannot tell us about the landscape. Sensors. 8(4), 2136–2160.

Jeevalakshmi, D., Narayana, R.S., Manikiam B., 2017. Land surface temperature retrieval from LANDSAT data using emissivity estimation.Int. J. of Applied Engineering Research. 12(20), 9679–9687.

Li, Z.L., Tang, B.H., Wu, H., Ren, H., Yan, G., Wan, Z., Trigo, I.F., Sobrino J.A., 2013. Satellite-derived land surface temperature: Current status and perspectives. Remote Sensing of Environment/ 131, 14–37.

Mallick, J., Kant, Y., Bharath, B.D., 2008. Estimation of land surface temperature over Delhi using Landsat-7 ETM+. J. Ind. Geophys. Union. 12 (3), 131–140.

Mkrtchian, O., 2016. Analysis of the relationships between morphometric relief parameters and visual characteristics of Ukrainian Carpathians ecosystems. Visn.Lviv. Univ. Ser. Geogr. 50, 249–256.

Mkrtchian, O., Shuber, P.M., 2009. Geoinformatsijne modeluvannia temperaturnoho polia zahidnykh rehioniv Ukrajiny [GIS modeling of the temperature field of the Western regions of Ukraine]. Phys. Geogr. and Geomorph. 57, 104–112 (in Ukrainian).

NASA, 2018. Landsat Science: Landsat 8 Overview. Retrieved from:

https://landsat.gsfc.nasa.gov/landsat-8/landsat-8-overview/

Oguz H., 2017. Automated land surface temperature retrieval from Landsat 8 satellite imagery: a case study of Diyarbakir – Turkey. Turkish Journal of Forest Science. 1(1), 33–43.

R Core Team, 2017. R: A language and environment for statistical computing. R Foundation for Statistical Computing, Vienna, Austria.Retrieved from: https://www.R-project.org/.

Sobrino, J.A., Jimenez-Munoz, J.C., Paolini, L., 2004.Land surface temperature retrieval from LANDSAT TM 5.Remote Sensing of Environment. 90, 434–440.

Sobrino, J.A., Jimenez-Munoz, J.C., Sòria, G., Romaguera, M., Guanter, L., Plaza, A., Martínez, P., 2008. Land surface emissivity retrieval from different VNIR and TIR Sensors. IEEE Transactions on Geoscience and Remote Sensing. 46 (2), 316–327.

Sobrino, J.A., Raissouni, N., 2010.Toward remote sensing methods for land cover dynamic monitoring: application to Morocco. International Journal of Remote Sensing. 21 (2), 353–366.

Vyshnevskyi, V.I., Shevchuk, S.A., 2017. Vykorystannia danyh dystantsijnoho zonduvannuia Zemli dla z'asuvannia termichnyh osoblyvostej Ukrajinskyh Karpat [Application of Earth remote sensing data to reveal the thermal features of Ukrainian Carpathians].Ukrainian journal of Earth remote sensing.12, 47–52 (in Ukrainian).

Xiaolei, Yu, Xulin, G, Zhaocong, Wu, 2014. Land surface temperature retrieval from Landsat 8 TIRS – comparison between radiative transfer equation-based method, split window algorithm and single channel method. Remote Sens. 6, 9829–9852.